from the relation

$$\xi = \pi - \cot^{-1}\left(\frac{H_e \sin\beta}{Z_e}\right) + \tan^{-1}\left\{\frac{A(X)_{max}}{S(X)_{max}} \cdot \frac{4\tan^{-1} B}{\ln\{(x_e - B)/(x_e + B)\}}\right\} \quad (3.84a)$$

or

$$\xi = \pi - \cot^{-1}\left(\frac{H_e \sin\beta}{Z_e}\right) + \tan^{-1}\left\{\frac{A(X)_{max}}{S(X)_{max}} \cdot \frac{4\tan^{-1} B}{\ln\{(x_{1/2} - B)/(x_{1/2} + B)\}}\right\}. \quad (3.84b)$$

Six master curves involving functions of d, b, and ξ for the symmetric and antisymmetric components of the dike profile are shown in Figure 3.26c. The dip-angle functions P and $\mathscr{P}$ in Figure 3.26 are related to known quantities in the following expansions of Equation (3.84):

$$\xi - \{\pi - \cot^{-1}(H_e \sin\beta/Z_e)\} = \tan^{-1}(\mathscr{A}P) \text{ or } \tan^{-1}(\mathscr{A}\mathscr{P}), \quad (3.85a)$$

where $\mathscr{A} = A(X)_{max}/S(X)_{max}$,

$$P = \frac{4\tan^{-1}(W/2D)}{\ln\{(1 - W)/(1 + W)\}}$$

$$\mathscr{P} = \frac{4\tan^{-1}(\mathscr{W}/2\mathscr{D})}{\ln\{(1 - \mathscr{W})/(1 + \mathscr{W})\}} \quad (3.85b)$$

Because Equation (3.83) gives W, D, $\mathscr{W}$, and $\mathscr{D}$ in terms of ϕ and μ, and these in turn can be found from the curves, P and $\mathscr{P}$ are fully determined.

We can solve for the total-field anomaly in similar fashion. The analysis for the dike of infinite depth extent has been extended to cover a prism of finite length and depth extent. Because of the extra terms, it is necessary to provide more master curves, but the procedure is similar. Master curves for other models are also availabele (Grant and Martin, 1966; Martin, 1966; Gay, 1967). The second reference contains the following models, in addition to the prism: horizontal slab, plate, rod, and dipping sheet. (The method can be extended to dikes or prisms in gravity interpretation.)

3.7.9. Matched Filtering

Where the problem is locating a signal in a data set, matched filtering provides a powerful method if the spectrum of the sought-for signal is known. A *matched filter* is a filter that has the same spectrum as the sought-for signal. One way to carry out matched filtering involves using the Hilbert transform (Sheriff and Geldart, 1983: §10.3.11) to separate the symmetric and antisymmetric anomaly components (§3.7.8). Both total-field and gradient data may be processed in this way (Naudy, 1971; Nabighian, 1984).

3.7.10. Werner Deconvolution

Werner (1953) proposed a method for isolating a magnetic anomaly from the interference produced by nearby anomalies. This led to automated procedures for interpreting magnetic data, now known as *Werner deconvolution* (Hartman, Teskey, and Friedberg, 1971; Jain, 1976; Kilty, 1983).

The magnetic anomaly for a dipping dike can be written in empirical form as

$$F(x) = \{M(x - x_0) + Nz\}/\{(x - x_0)^2 + z^2\} \quad (3.86a)$$

where x_0 is the surface point directly above the center of the top of the dike, z is the depth to the top, x is the point of measurement, and the x axis is normal to the strike. M and N are unknown functions of the dike geometry and mineralization. Rearranging Equation (3.86a) in the form

$$x^2F(x) = a_0 + a_1x + b_0F(x) + b_1xF(x) \quad (3.86b)$$

where $a_0 = -Mx_0 + Nz$, $a_1 = M$, $b_0 = -x_0^2 - z^2$, and $b_1 = 2x_0$, we find that $x_0 = b_1/2$ and $z = (-4b_0 - b_1^2)^{1/2}/2$. Thus we can determine x_0 and z by measuring F at four stations and solving Equation (3.86b) for a_0, a_1, b_0, and b_1.

Extending the problem beyond an isolated anomaly. Werner assumed that the noise or interference caused by neighboring magnetic anomalies could be taken into account by extending the polynomial, so that the measured field $\mathscr{F}$ becomes

$$\mathscr{F} = F(x) + c_0 + c_1x + \cdots + c_nx^n \quad (3.87)$$

where $F(x)$ is given by Equation (3.86a) so that $(n + 5)$ unknown quantities are involved. Usually the polynomial is first or second order only, so that six or seven stations are sufficient for a solution.

The scope of this analysis has been enlarged to include models other than dikes: basement topography, magnetic interfaces (which use dF/dx rather

Table 3.3. *Empirical depth estimation methods for magnetic anomalies.*

Method	Half-width	Peak-to-Zero	Vertical grad.	Flank slope
Component measured	F, Z	F, Z, H	$F, \partial F/\partial z$, $Z, \partial Z/\partial z$	F, Z
Model				
Monopole	$1.3x_{1/2}$	$1.3x_{p0}$	$-2F/(\partial F/\partial z)$	
Dipole	$2x_{1/2}$	$1.3/x_{p0} \leq 2$	$-3F/(\partial F/\partial z)$	
Monopole line	$x_{1/2}$	x_{p0}	$-F/(\partial F/\partial z)$	
Dipole line	$2x_{1/2}$	x_{p0}	$-2F/(\partial F/\partial z)$	
General	$0.7 \leq x_{1/2} \leq 1.3$	x_{p0}	$-nF/(\partial F/\partial z)$	$0.5 \leq x_f \leq 1.5$

Note: $x_{1/2}$ is the full width at half-peak amplitude, x_{p0} is the horizontal distance from peak to zero-crossing, n is an empirically determined index factor, and x_f is the horizontal distance over which slope is straight line.

than F), faults, and contacts. This type of analysis is also suitable for gravity interpretation.

There are limitations to Werner deconvolution, such as resolution between neighboring bodies and lack of discrimination among parameters, leading to a relation between, say, dip angle and susceptibility. The data are sensitive to geological and measurement noise (signal/noise = 100 produces 20% scatter in depth and position estimates). However, the technique is attractive because of ease of access to the computer and consequent speed in handling large quantities of data.

3.7.11. Depth Estimates

(a) Smith rules for maximum depth. As in Section 2.7.12, which dealt with depth estimates for gravity anomalies, there are corresponding limiting values in magnetics derived by Smith (1961). If the magnetization M is parallel throughout a body, though not necessarily uniform or even in the same sense, and if $|M|_{max}$, $|\partial Z/\partial x|_{max}$, and $|\partial Z^2/\partial x^2|_{max}$ are absolute values of the maxima of M and the first and second derivatives of F or Z along the x profile, then the depth z_u to the upper surface is given by

$$\left.\begin{aligned} z_u &\leq 5|M|_{max}/|\partial F/\partial x|_{max} \\ z_u^2 &\leq 30|M|_{max}/|\partial F^2/\partial x^2|_{max} \end{aligned}\right\} \quad (3.88a)$$

For Z profiles, where M is everywhere vertical and in the same direction (down or up), the numerical factors are reduced to 2.6 and 3.1, respectively.

For two-dimensional magnetic features having infinite length in the y direction, in which the total magnetization is parallel throughout, the equivalent expressions become

$$\text{and} \qquad \left.\begin{aligned} z &\leq 4|M|_{max}/|\partial F/\partial x|_{max} \\ z^2 &\leq 5|M|_{max}/|\partial F^2/\partial x^2|_{max} \end{aligned}\right\} \quad (3.88b)$$

Where the body is uniformly magnetized by induction, we may replace M_{max} by kF_e or $kF_e/(1 + Nk)$ as in Equation (3.67).

Because we do not normally have a value of M_{max}, estimates obtained by combining the two limits are even cruder than the equivalent relations for gravity. For a semiinfinite thin sheet, the result is within 50%, but it appears to be even poorer for three-dimensional features.

(b) Empirical depth rules. A number of rules-of-thumb for depth estimation have developed from practical experience in magnetic interpretation. These relate to profile shapes; for example, they often use horizontal widths at some fraction of the peak value for symmetrical curves and horizontal distances from peak-to-zero values for asymmetric curves. Peters (1949) was probably the first to relate depth to the horizontal extent of portions of sloping flanks, and variations of slope techniques are among the most popular. The vertical gradient is also used in such rules (Barongo, 1985). A summary of such rules is given in Table 3.3.

Slope methods are widely used, especially for aeromagnetic interpretation. Graphical techniques use the sloping flanks of profiles to estimate depth (Nettleton, 1971; Spector, 1979). In Figure 3.27a, S is the horizontal extent of the portion of the curve that is nearly linear at the maximum slope. Two additional line segments have been drawn tangent to the profile at half the maximum slope; the distance between the points of tangency is P. The depth of the source beneath these portions of the curve is given by

$$h = k_1 S \qquad 1.67 \leq k_1 \leq 2.0$$
$$(\text{generally } k_1 \approx 1.82) \quad (3.89a)$$
$$h = k_2 P \quad (\text{generally } k_2 \approx 0.63) \quad (3.89b)$$

The use of both methods provides a check on the

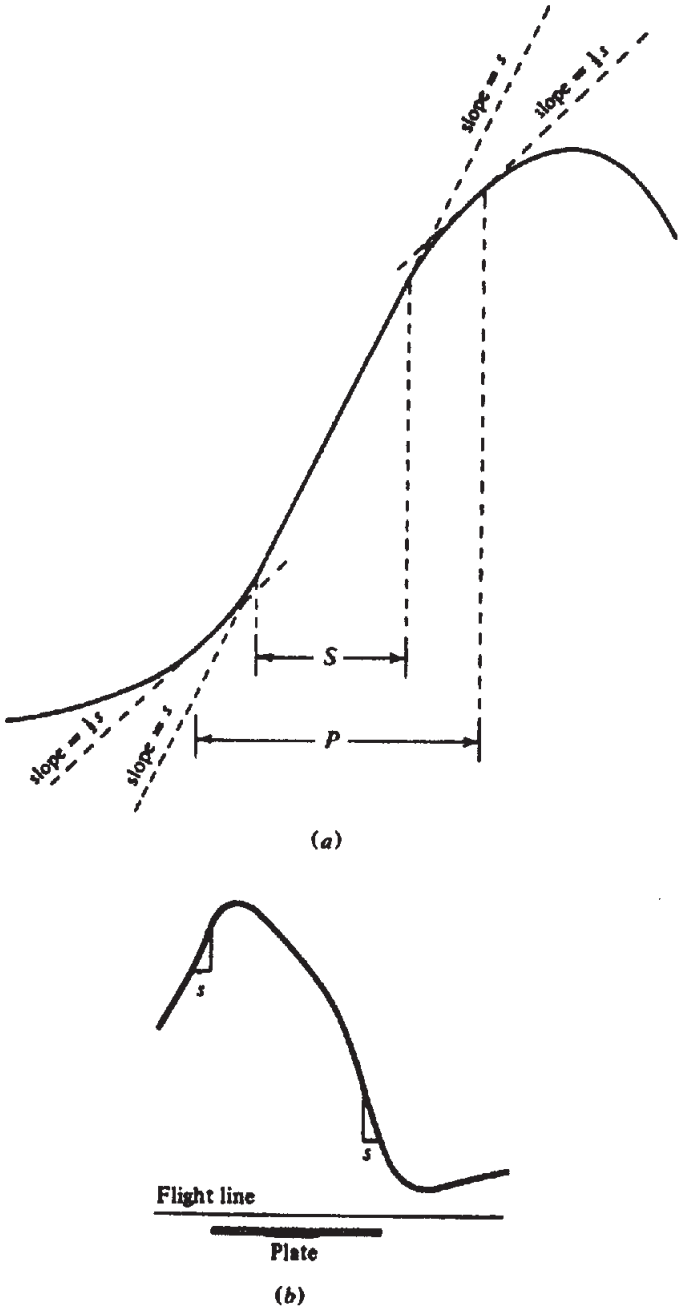

Figure 3.27. Determining anomaly depth from the slope of a magnetic profile. (a) Maximum-slope (S) and half-slope (P) measurements. (b) Maximum-slope measurements on a thin plate anomaly.

depth estimates and the care with which the graphical analysis is done. This method generally yields reasonable results for horizontal basement models with steeply dipping contacts; thus, it is suitable in the analysis of airborne data. It is much simpler and faster and provides more depth estimates than analysis by model curve fitting. It can be carried out on original field profiles and so need not wait on map preparation; it can also be applied to analysis of maps (Rao and Babu, 1984).

Use of slope techniques requires corrections. When flight lines are not normal to the local geological strike, horizontal distances are too large and should be multiplied by a cosine factor. Correction also has to be made for the flight elevation to give values with respect to sea level (or to an arbitrary datum).

3.8. FIELD EXAMPLES

3.8.1. Ground Surveys

(1) The first example shows the inherent complexity of ground magnetic data and the difficulties in accurately interpreting them. Figure 3.28 displays magnetic contours and two vertical component profiles

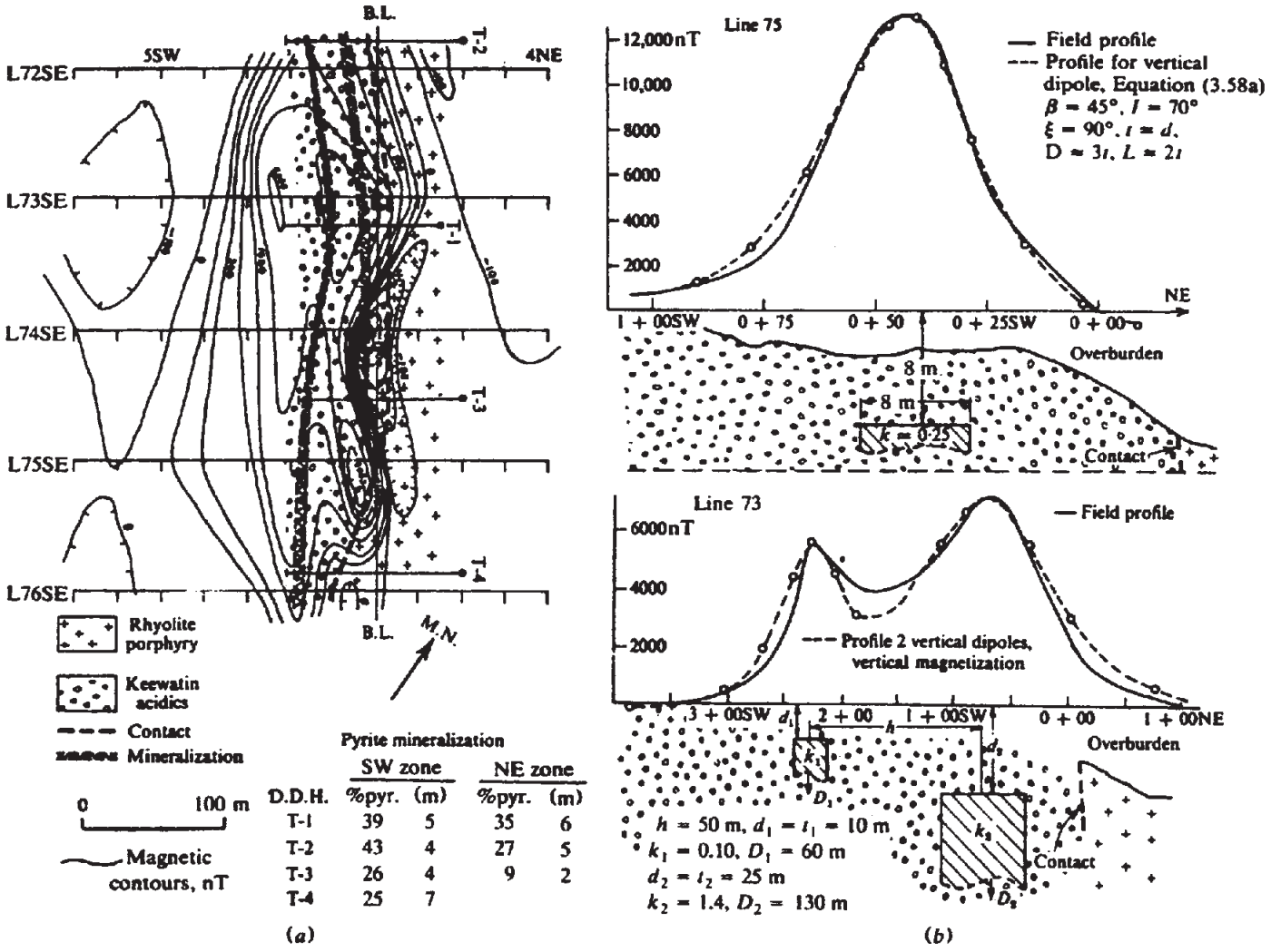

Figure 3.28. Ground magnetic survey over pyrite mineralization, Barraute, northwest Quebec. (a) Magnetic map. (b) Attempt to match profiles on lines 75SE and 73SE.

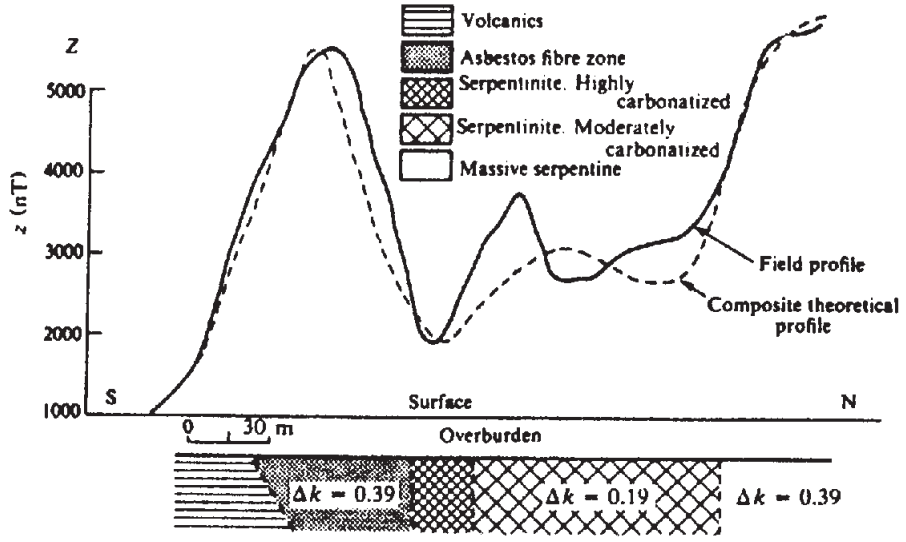

Figure 3.29. Vertical component ground magnetic profile in an area of asbestos mineralization near Matheson, Ontario.

normal to the strike of pyrite mineralization. There are two parallel pyrite zones in acidic flows, near a contact between the latter and rhyolite porphyry. Both have a strike length greater than 300 m and the zone nearer the contact appears to pinch out on line 75.

Although the pyrite mineralization is clearly associated with a magnetic trend in the area, the large magnetic anomalies on lines 73 and 75 could only be due to magnetite or possibly pyrrhotite, since the susceptibility of pyrite is relatively low (Table 3.1). However, there is no specific indication of these minerals in the drill logs of holes 1 to 4.

Because the overburden near the diamond drill holes was generally quite thick (25 m at T-1, for example), it was originally assumed to be at least 15 m throughout the grid. However, a shallow seismic refraction survey carried out later on line 75 showed bedrock only 1.5 to 3 m below the surface in the vicinity of the pyrite zones, dropping off abruptly to 15 to 25 m northeast of the acidic flow–rhyolite contact. Thus the magnetite sources may be very close to the surface and of small depth extent.

The source for the single 13 μT peak on line 75 appears to be a finite steeply dipping sheet at very shallow depth. Using Equation (3.58a) with $\beta = 45°$, $I = 70°$, $\xi = 90°$, and $Z_e = 36$ μT, and fitting the profiles at three points (including the maximum), we obtain a reasonable fit with $t \approx d \approx 8$ m, $D \approx 25$ m, $2L \approx 30$ m, and $k = 3$ SI unit (See Fig. 3.28b). However, when we try to match the double peak profile on line 73 by assuming two vertical sheets of identical cross section separated by 50 m and inductively magnetized in the earth's field, Equation (3.58a) produces the following parameters: $d \approx t = 2.5$ m, $D = 70$ m, $2L = 90$ m, $k_1 = 1.3$ SI, and $k_2 = 1.9$ SI. This results in a reasonable match of the central trough and the northeast flank, but the southwest flank is much too large. A better fit (shown in Fig. 3.28b) was obtained with the two vertical sheets illustrated, but the trough between them is too deep. Also, the depth extent must be less than 120 m because the bodies were not encountered in holes T-1 and T-3. Although this interpretation is certainly not definitive, it is clear that the magnetic sources are shallow, have limited strike length, steep dip, and large susceptibility contrast. This last fact indicates high magnetite content and possibly large remanence, which may be responsible for the disagreements (Green, 1960).

(2) The magnetic method is particularly useful in exploring for asbestos because of its occurrence in ultrabasic intrusive rocks rich in magnetite. When olivine (Mg_2SiO_4) is altered to serpentine ($Mg_3SiO_5(OH)_4$) and magnesite ($MgCO_3$) by the addition of water and carbon dioxide, the asbestos is associated with high magnetic susceptibility and massive serpentinite. Figure 3.29 shows a vertical component profile over an asbestos prospect near Matheson in northern Ontario and the geologic section under a 15 m overburden. High magnetic responses correspond to the asbestos and massive serpentine zones with lows over the volcanics and highly carbonized serpentite. A reasonable match to the field profile was obtained by assuming dikes of considerable depth extent using Equation (3.44a) with $r_2 \approx r_4$, $\phi_2 \approx \phi_4$, $\beta = \pi/2$, and all contacts vertical except the left one, which dips 30°. The presence of asbestos in the massive serpentine zones can only be established by drilling.

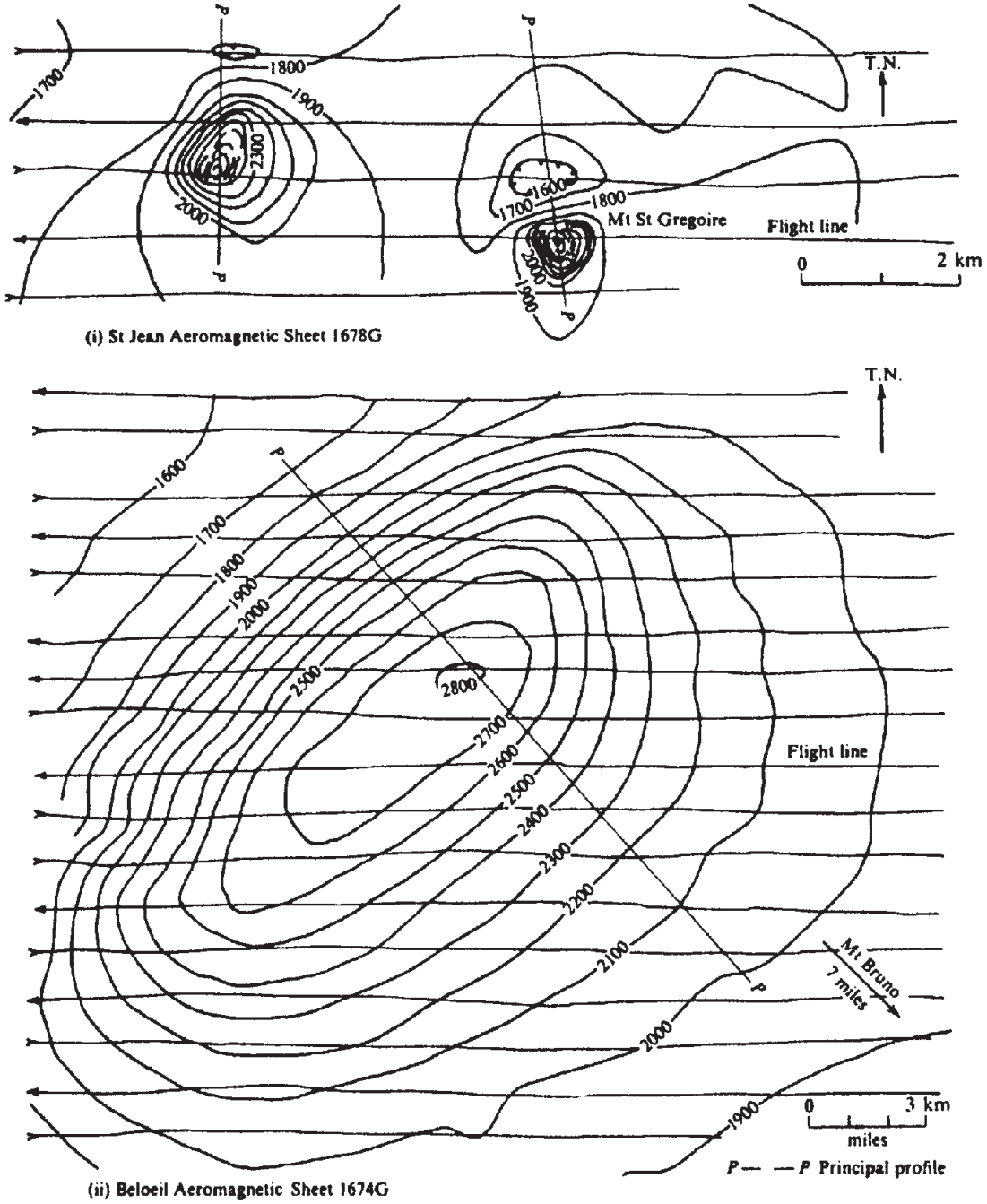

Figure 3.30. Magnetic data for three anomalous areas in the St. Lawrence lowlands. (a) Maps, C.I. = 100 nT.

3.8.2. Airborne Surveys

(1) The Monteregian hills of the St. Lawrence lowland region near Montreal were formed by igneous intrusions into sedimentary rocks. These hills are magnetic as well as topographic anomalies because of their contrast with the low susceptibility sediments. Aeromagnetic maps (Canadian Government Aeromagnetic Series, St. Jean and Beloeil) show this clearly for Mt. Bruno, Mt. St. Hilaire, Mt. Rougemont, and Mt. St. Gregoire. On the same sheets we also see two well-defined magnetic highs that are not topographic features: one about 5 km west of Mt. St. Gregoire and a larger one 11 km northwest of Mt. Bruno. One assumes that they are igneous plugs that failed to reach the eminence of the Monteregian hills.

These two features and Mt. St. Gregoire provide excellent examples of the vertical-prism model commonly employed in aeromagnetic interpretation. Figure 3.30a shows the total-field contours, whereas profiles are displayed in Figure 3.30b. Two methods